

Max-Planck-Institut
für Mathematik
in den Naturwissenschaften
Leipzig

Interacting tails of asymmetric domain walls
theory and experiments

by

Lukas Döring, Claudia Hengst, Felix Otto, and Rudolf Schäfer

Preprint no.: 14

2015



Interacting tails of asymmetric domain walls – theory and experiments

Lukas Döring*

RWTH Aachen, Lehrstuhl I für Mathematik, Pontdriesch 14-16, 52056 Aachen, Germany

Claudia Hengst

IFW Dresden, Institute for Complex Materials, PO 270116, 01171 Dresden, Germany

Felix Otto

*Max Planck Institute for Mathematics in the Sciences, Inselstraße 22, 04103 Leipzig, Germany and
Universität Leipzig, Mathematisches Institut, PF 100920, 04009 Leipzig, Germany*

Rudolf Schäfer

*IFW Dresden, Institute for Metallic Materials, PO 270116, 01171 Dresden, Germany and
Dresden University of Technology, Institute for Materials Science, PO 01062 Dresden, Germany*

(Dated: February 18, 2015)

In this paper, we address the structure and interaction of neighboring asymmetric Néel and Bloch walls in soft ferromagnetic films.

First, we review a recent reduced model for the structure of parallel systems of asymmetric walls with potentially interacting tails. The reduced model has the form of a minimization problem in two parameters that describe the amount of rotation in a stray-field free wall-core and the average hard-axis magnetization in each domain, respectively. Starting from the micromagnetic torque equation, we provide a new derivation of this reduced model that uses the method of matched asymptotic expansions instead of the original variational approach. The theoretical results apply to any soft thin-film material and cover also isolated domain walls, in the limiting case of large domain widths.

With only little numerical effort, we then obtain detailed quantitative information on the structure of asymmetric domain walls. In particular, we predict the hard-axis magnetization curves for asymmetric Bloch and interacting asymmetric Néel walls.

In the second part of the paper, we report on experimentally observed domain-wall transitions in $\text{Co}_{40}\text{Fe}_{40}\text{B}_{20}$ films of lateral dimensions $60\mu\text{m} \times 9500\mu\text{m}$ and thicknesses 102nm, 153nm, and 212nm. Upon the wall transition, the average hard-axis magnetization in the domains increases significantly. The increase depends on the width of the domains and ranges from $0.1M_s$ to $0.25M_s$ for domain widths between $18\mu\text{m}$ and $6\mu\text{m}$. For the thicknesses 102nm and 153nm, the predicted hard-axis magnetization jump excellently agrees with the experimental data. We conclude that interacting tails of neighboring asymmetric Néel walls cause the observed additional rotation of the magnetization towards large hard-axis fields.

Hence, our results contribute to a quantitative understanding of isolated and interacting asymmetric domain walls in soft ferromagnetic films.

I. INTRODUCTION

Even though magnetic domain walls in ferromagnetic films have been under experimental and theoretical investigation for a long time, a general theory that describes their properties and structure is not yet available. Depending on the film thickness, the magnetic properties of the material and applied magnetic fields, different wall types may be energetically favored. Figure 1 shows a phase diagram that indicates the wall type of least energy in films of Permalloy and CoFeB, depending on the normalized film thickness t/d and the reduced field $H = \frac{|\vec{H}|}{H_K}$, for the two material-dependent quality factors $Q = \frac{K_u}{K_d}$. Here, H_K denotes the anisotropy field, K_u the first-order anisotropy constant, $d = \sqrt{A/K_d}$ the Bloch line width, A the exchange constant and $K_d = \frac{1}{2}\mu_0 M_s^2$ the demagnetizing constant of the material with the vacuum permeability μ_0 and the saturation magnetization M_s . In this

work, we will only consider soft materials, i.e. $Q \ll 1$.

In very thin films, symmetric Néel walls are observed with a magnetization profile that splits into a narrow core region with an extension of the order of $\sim d^2/t$ and extended tails with a logarithmically decaying magnetization over a width $w_{\text{tails}} \sim t/Q$. For low-anisotropy materials, the dominant contribution to the energy of symmetric Néel walls is the stray field generated in their tails.

For intermediate film-thicknesses, cross-tie walls are observed which consist of a series of Bloch lines and 90° Néel wall segments in between. Note that the results presented below do not allow for a prediction of the cross-tie wall energy, which is therefore not present in the phase diagram.

In thicker films, partially or completely stray-field free domain walls are energetically favored, namely the asymmetric Néel wall and asymmetric Bloch wall.^{2,3} In contrast to the asymmetric Bloch wall, the asymmetric Néel

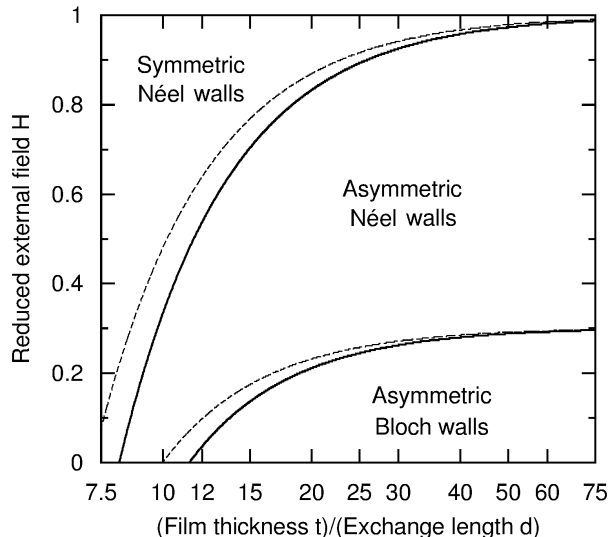


Figure 1. Phase diagram according to (5) for nanocrystalline Permalloy and amorphous CoFeB, i.e. $Q = 2.5 \cdot 10^{-4}$ (solid lines) and $Q = 1.55 \cdot 10^{-3}$, respectively. Note that compared to Ref. 1, Fig. 3.80, the transition between symmetric and asymmetric Néel walls is shifted towards larger fields.

wall reduces its energy by splitting off an extended tail. A vortex pattern is formed within the wall core, which avoids most of the dipolar charge. Typically, about 10% of the dipolar charges are distributed in the tails of asymmetric Néel walls. With increasing hard-axis field the contribution of the tails to the total magnetization rotation increases until – at a critical field value – the asymmetric core disappears in favor of a symmetric Néel wall structure (cf. Ref. 1, Section 3.6.4 (E)). For a more detailed review on magnetic domain walls in thin films we refer the reader to Ref. 1 and references therein.

The existence of different wall types as well as the occurrence of domain wall transitions in an applied field is of practical relevance for various applications. For instance it has been shown recently that the high-frequency magnetization response of domain structures is significantly altered due to a network of interacting neighboring walls.⁴ As the acoustic domain resonance frequency depends on the effective domain wall width and on the interaction strength between neighboring domain walls, either smooth or step-like changes (in the order of 0.5 GHz) of the domain resonance frequency can be observed due to domain wall transformations. For the quantification of such effects, the knowledge of the internal structure of a domain wall, i.e. its width and the strength of interaction with walls in the neighborhood is indispensable.

The interaction between neighboring symmetric Néel walls by an overlap of their extended tails has been demonstrated to significantly determine the energy balance and structure of the domain walls.¹ Whereas wall interaction does not play a dominant role for stray-field free asymmetric Bloch walls, it can be still significant for

the energy and magnetization configuration of neighboring asymmetric Néel walls.

The analysis of domain walls very much depends on the specific wall type: On the one hand, the one-dimensional nature of symmetric Néel walls makes both their numerical⁵ and analytic^{6–9} treatment possible. On the other hand, the structure of asymmetric Bloch walls is only accessible to Ritz methods^{2,3} or numerical micromagnetics^{10,11}, which is feasible due to the small wall width. For asymmetric Néel walls, the combination of a two-dimensional wall pattern with long-range extended tails makes this type of wall difficult to study by numerical simulation^{1,11}.

Recently, a step towards a quantitative understanding of the splitting of asymmetric Néel walls into stray-field free core and logarithmic tails has been undertaken. In Ref. 12 an asymptotic limit of the micromagnetic energy functional was derived that yields a precise description of the relative amount of rotation in stray-field free core and logarithmic wall tails for an isolated domain wall. The results have been generalized to systems of interacting domain walls.¹³

Here, we briefly summarize the main results of Refs. 12 and 13 and compare the theoretical with experimental results for $\text{Co}_{40}\text{Fe}_{40}\text{B}_{20}$ films. Thereby we aim to demonstrate the validity of the proposed model, which can be easily applied for various magnetic thin film materials. Additionally, we provide an alternative derivation of the reduced models that focuses on the torque balance between magnetic moments and effective field instead of energy considerations.

II. THEORY

Consider a ferromagnetic film with uniaxial anisotropy ($\parallel y$), a thickness t with $-\frac{t}{2} \leq z \leq \frac{t}{2}$ and infinite extensions in the film plane (xy -plane). For the presence of magnetic domain walls in the film two cases will be distinguished, as sketched in Fig. 2.

In a first case (a) we assume that two domains of constant magnetization $\vec{m}(x = \pm\infty) = (\cos \alpha, \pm \sin \alpha, 0)$ have formed and are separated by a domain wall. Then, in a second case (b) a system of domain walls is considered that are equally spaced at a distance w and which may interact via extended wall tails. The energy of isolated and interacting domain walls in an external field $\vec{H}_{\text{ext}} \parallel x$ is derived starting from the Landau-Lifshitz energy (see, e.g., Ref. 1, Section 3.2):

$$\begin{aligned} \mathbb{E} = A \int |\text{grad } \vec{m}|^2 dV - \frac{1}{2} \mu_0 M_s \int \vec{H}_d \cdot \vec{m} dV \\ + K_u \int (1 - (\vec{m} \cdot \vec{e})^2) dV - \mu_0 M_s \int \vec{H}_{\text{ext}} \cdot \vec{m} dV, \end{aligned} \quad (1)$$

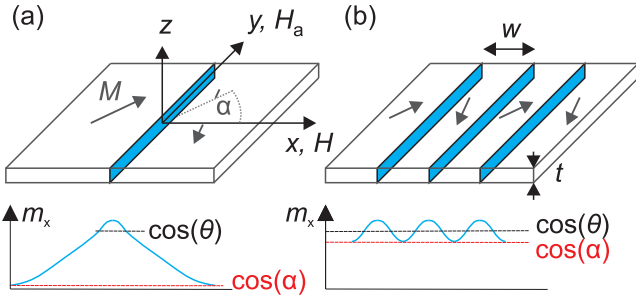


Figure 2. (Color online) Domain configuration (top) considered in the reduced model for (a) an isolated domain wall (blue) and (b) a system of domain walls at distance w in an extended film of thickness t . The bottom row *schematically* illustrates the magnetization component m_x on the film surface with core ($m_x > \cos \theta$) and tail region ($m_x > \cos \alpha$) of asymmetric walls.

with the magnetization vector $\vec{m} = \frac{\vec{M}}{M_s}$, the stray or demagnetizing field \vec{H}_d , and $\vec{e} \parallel y$ the anisotropy axis. By dV we denote the volume element.

To make the problem accessible to a mathematical treatment, we assume that all domain walls are parallel to the y -axis and the magnetization configuration is translation invariant in y , so that it suffices to study the energy density per length in the y -direction. Note, however, that this assumption excludes the formation of Bloch lines and wall segmentation as it occurs for cross-tie walls.

A. A reduced model for domain walls in moderately thin films

In order to reduce the number of physical parameters in the problem, we employ the K_d -based non-dimensionalization¹⁴ of (1). On a cross-section of the sample in the xz -plane with area element dA we obtain:

$$E = d^2 \int |\text{grad } \vec{m}|^2 dA + \int_{\mathbb{R}^2} |\vec{h}_d|^2 dA + Q \int ((m_x - H)^2 + m_z^2) dA, \quad (2)$$

with $\vec{H}_d = M_s \vec{h}_d$ and $\vec{H}_{\text{ext}} = H_K(H, 0, 0) = M_s Q(H, 0, 0)$. The quantity H denotes the reduced external field. Note that while passing from (1) to (2) we have also added the normalizing constant $Q \int H^2 dA$ to ensure that each of the constant magnetization configurations $\vec{m} = (H, \pm\sqrt{1-H^2}, 0)$ has vanishing energy density. Moreover, E is only partially non-dimensional and has units of area.

In the regime $Q \ll (\frac{t}{d})^2 \ll Q^{-1}$ and for a wall angle $2\alpha = 180^\circ$, the minimal wall energy (2) per unit domain wall length is known¹⁵ to scale as follows (up to a multi-

plicative constant):

$$E_{\text{wall}} \sim \begin{cases} t^2 \ln^{-1} \frac{1}{Q}, & \text{if } (\frac{t}{d})^2 \leq \ln \frac{1}{Q}, \\ d^2, & \text{if } (\frac{t}{d})^2 \geq \ln \frac{1}{Q}. \end{cases}$$

In thin films, the minimal-energy scaling $E_{\text{wall}} \sim \frac{\pi}{2} t^2 \ln^{-1} \frac{1}{Q}$ is satisfied by symmetric Néel walls (see also Refs. 14, Section 4.6.2, and 7). In thicker films, the minimal-energy scaling $E_{\text{wall}} \sim d^2$ is satisfied by, e.g., a stray-field free asymmetric Bloch wall.

Thus, in order to analyze both symmetric and asymmetric walls, in particular asymmetric Néel walls with extended tails, it seems most promising to focus on the critical regime of the cross-over from symmetric to asymmetric wall types, i.e. the asymptotic regime $(\frac{t}{d})^2 \sim \ln \frac{1}{Q}$ as $Q \downarrow 0$. In this regime, for sufficiently large (reduced) hard-axis field $H \in [0, 1]$, one expects to recover a domain wall of Néel instead of Bloch type.

In Refs. 12 and 13, it has been shown mathematically rigorously that in this regime and both for isolated and interacting walls the internal structure of an arbitrary domain wall can be determined by analyzing a simple scalar minimization problem.

We will describe the result for the periodic case (b): One may assume that the width $w \gg t$ of the domains is strictly smaller than the width t/Q of the tails of symmetric Néel walls that are constrained only by anisotropy. Otherwise, one does not expect interaction of the walls and may treat each domain wall independently. In particular, for $w \ll t/Q$ it is expected that the wall tails invade the whole domain. Thus, to leading order in $w/t \uparrow \infty$, the sum of stray-field and anisotropy/Zeeman energy of logarithmic wall tails that connect the magnetization $m_x = \cos \theta$ in the core to $m_x = \cos \alpha$ in the center of a domain (cf. Fig. 2) is given by

$$E_{\text{tails}}(\theta, \alpha, H) := \frac{\pi}{2} t^2 \frac{(\cos \theta - \cos \alpha)^2}{\ln \frac{w}{t}} + Qwt(\cos \alpha - H)^2.$$

Optimizing the angle α , we find that the magnetization in the center of the domain is given by

$$\cos \alpha_{\text{opt}} = H + \frac{\pi t}{\pi t + 2Qw \ln \frac{w}{t}} (\cos \theta - H). \quad (3)$$

In particular, one identifies the interesting regime of periods

$$w \sim \frac{t}{Q \ln(1/Q)},$$

in which a non-trivial $\cos \alpha$ is possible. Surprisingly, the domain width w needs to be by $\ln(1/Q)$ smaller than the naive guess t/Q for the critical regime of periods.

The optimal angle θ for the transition from stray-field free wall core to the logarithmic tails under the reduced external field H can be found by optimizing the sum of the minimal exchange energy $E_{\text{core}}(\theta)$ of a stray-field free

wall core¹⁶ of wall angle θ and the energy of the optimal wall tails:

$$E_{\text{wall}}(H) \approx \min_{\theta} \left(E_{\text{core}}(\theta) + \underbrace{\min_{\alpha} E_{\text{tails}}(\theta, \alpha, H)}_{= \frac{\pi}{2} t^2 \frac{2Qw}{\pi t + 2Qw \ln \frac{w}{t}} (\cos \theta - H)^2} \right). \quad (4)$$

Choosing¹⁷ $w \gg t/Q \ln \frac{1}{Q}$, one recovers for $Q \ll 1$ a reduced model for the structure of an isolated domain wall (a):

$$E_{\text{wall}}(H) \approx \min_{\theta} \left(E_{\text{core}}(\theta) + \frac{\pi}{2} \frac{t^2}{\ln \frac{1}{Q}} (\cos \theta - H)^2 \right). \quad (5)$$

The structure of (4) and (5) confirms and quantifies the description of asymmetric Néel walls as an optimal combination of stray-field free wall cores with extended tails given in Ref. 1, Section 3.6.4 (E). In other words, the above results demonstrate that asymmetric Néel walls have two internal parameters – the core and domain wall angles θ and α – that the wall optimizes automatically to produce the lowest micromagnetic energy given a reduced external field H .

Note that this explanation (and also the rigorous proof in Refs. 12 and 13) takes an *energetic* point of view and is precise only in the limit $Q \downarrow 0$. In the following section, we will demonstrate that asymptotically the same result (4) can be derived starting from the micromagnetic equations in the form of a *torque balance*, using the method of matched asymptotic expansions. Moreover, this approach potentially yields slightly more precise quantitative results for positive $0 < Q \ll 1$.

B. Matching core and tails by asymptotic expansions

We will focus on the periodic case (b): Starting point in the method of matched asymptotic expansions is the first variation of the micromagnetic energy in its non-dimensionalized form (2)

$$\vec{m} \times \left(-d^2 \Delta \vec{m} - \vec{h}_d + Q \begin{pmatrix} m_x - H \\ 0 \\ m_z \end{pmatrix} \right) = 0 \quad \text{for } |z| < \frac{t}{2}, \\ \partial_z \vec{m} = 0 \quad \text{for } |z| = \frac{t}{2}. \quad (6)$$

This torque balance has to be supplemented by (quasi-static remnants of) Maxwell's equations, expressed in terms of the stray-field potential u (that is, $h_d = -\text{grad} u$):

$$\begin{aligned} \Delta u &= \text{div} \vec{m} \quad \text{for } |z| < \frac{t}{2}, \\ [-\partial_z u] &= m_z \quad \text{for } z = \pm \frac{t}{2}, \\ \Delta u &= 0 \quad \text{for } |z| > \frac{t}{2}. \end{aligned} \quad (7)$$

We will assume that the configuration has the symmetry of the asymmetric Néel wall, i.e. that it is invariant under

the transformation $(x, z) \rightarrow -(x, z)$, $m_y \rightarrow -m_y$, $u \rightarrow -u$ at each wall core.

We first turn to the core or *inner* region in the parlance of matched asymptotics. Because this region is small, it can afford a z -dependent magnetization pattern that to leading order avoids magnetic charges. Likewise, the effects of anisotropy and external field are negligible. Hence in this region, (6) and (7) are well-approximated by

$$\left. \begin{aligned} \vec{m}_{in} \times \left(-\Delta \vec{m}_{in} + \text{grad} \frac{u_{in}}{d^2} \right) &= 0 \\ \text{div} \vec{m}_{in} &= 0 \end{aligned} \right\} \quad \text{for } |z| < \frac{t}{2}, \quad (8)$$

$$\partial_z(m_{in,x}, m_{in,y}) = 0 \quad \text{and} \quad m_{in,z} = 0 \quad \text{for } |z| = \frac{t}{2}.$$

In the first equation, the (reduced) stray-field potential $\frac{u_{in}}{d^2}$ plays the role of a Lagrange multiplier for the divergence-free condition in the second equation, like the pressure in the equations describing an incompressible fluid. We learn from (8) that the only length scale for the core is the film thickness t . For all physically relevant solutions of (8), the asymptotic behavior (i.e. for large $|x|$) of the magnetization \vec{m}_{in} is of the form

$$\vec{m}_{in} \approx (\cos \theta, \pm \sin \theta, 0) \quad \text{for } \pm x \gg t \quad (9)$$

for *some* angle θ , which we interpret as the amount of magnetization rotation in the asymmetric core. In fact, there are two and only two continuous branches $\theta \mapsto \vec{m}_{in,\theta}$ of solutions of (8) with (9) that correspond to the core of an asymmetric Néel (as opposed to Bloch) wall. Both are related by a reflection $z \rightarrow -z$, $m_z \rightarrow -m_z$ and hence have the same energy. They intersect only for the angle $\theta = 0$, where $\vec{m}_{in,\theta} = (1, 0, 0)$. Under smooth changes of the external field H , the relevant solutions will be on the same branch, which effectively makes the relevant $\vec{m}_{in,\theta}$ uniquely defined. In line with the discussion that leads to the approximation (8), the energy of $\vec{m}_{in,\theta}$ is given by

$$E_{\text{core}}(\theta) = d^2 \int |\text{grad} \vec{m}_{in,\theta}|^2 dA. \quad (10)$$

This now allows to characterize the asymptotic behavior also of the stray-field potential u :

$$4t(\sin \theta) u_{in} \approx \pm \frac{dE_{\text{core}}}{d\theta} \quad \text{for } \pm x \gg t. \quad (11)$$

We note that (11) follows from using (9) after integrating in x the identity

$$\begin{aligned} \frac{d}{d\theta} \frac{1}{2} \int_{-\frac{t}{2}}^{\frac{t}{2}} |\text{grad} \vec{m}_{in,\theta}|^2 dz \\ = \frac{d}{dx} \int_{-\frac{t}{2}}^{\frac{t}{2}} (\partial_x \vec{m}_{in,\theta} \cdot \partial_\theta \vec{m}_{in,\theta} - \frac{u_{in}}{d^2} \partial_\theta m_{in,\theta,x}) dz, \end{aligned}$$

which belongs to the realm of equipartition of energy statements and easily follows from multiplying (8) with $\partial_\theta \vec{m}_{in,\theta}$.

In the large tail region, the *outer* region, we neglect variations of the magnetization in the z direction, neglect the m_z -component, and project all the magnetic charges into the $\{z = 0\}$ -plane, so that (7) turns into

$$\begin{aligned} \partial_z u_{out}(z = 0^+) - \partial_z u_{out}(z = 0^-) \\ = \underbrace{t \partial_x (m_{out,x} - H)}_{= t \partial_x m_{out,x}} \text{ for } z = 0, \\ \Delta u_{out} = 0 \text{ for } z \neq 0, \end{aligned} \quad (12)$$

where we denote by $z = 0^+$ and $z = 0^-$ the limits $z \rightarrow 0$ with $z > 0$ and $z < 0$, respectively, i.e. the limits from above and below.

On the other hand, in the in-plane projection of the torque balance $\vec{m} \parallel -d^2 \Delta \vec{m} - \vec{h}_d + Q((m_x - H)\vec{e}_x + m_z \vec{e}_z)$, cf. (6), we neglect the exchange term and arrive at $(m_x, m_y) \parallel (\partial_x u + Q(m_x - H), \partial_y u = 0)$, which, as long as $m_y \neq 0$, i.e. away from the wall cores, implies¹⁸

$$\partial_x u_{out} + Q(m_{out,x} - H) = 0 \text{ for } z = 0, x \notin w\mathbb{Z}. \quad (13)$$

We note that (12) & (13) form a system of *linear* equations for $(u_{out}, m_{out,x} - H)$, with a one-dimensional set of physically relevant solutions. The two relevant length scales are w and t/Q . It is also convenient to choose the multiplicative degree of freedom A_{out} such that it normalizes the near-field behavior

$$u_{out} = \pm A_{out} \text{ for } z = 0 \text{ and } x = 0^\pm, \quad (14)$$

periodically extended.

Equating the inner and outer approximation to the stray-field potential, that is, u_{in} from (11) and u_{out} from (14), in the intermediate region $t \ll x \ll w$ yields the first matching condition

$$A_{out} = \frac{1}{4t \sin \theta} \frac{dE_{core}}{d\theta}. \quad (15)$$

The second matching condition comes from equating the magnetizations: The Fourier transform of the solutions of (12) & (13) can be determined explicitly. For fixed $m_{out,x}$, equation (12) is solved by

$$\mathcal{F}(u_{out})(k, z) = -t \frac{\mathcal{F}(\partial_x (m_{out,x} - H))(k, z)}{2|k|} e^{-|k||z|}, \quad k \in \frac{2\pi}{w}\mathbb{Z}.$$

Multiplying (13) by e^{-ikx} , integrating the result in x on $[0, w)$ and using the above, one finds

$$\mathcal{F}(m_{out,x} - H)(k) = \frac{2A_{out}}{Q + \frac{t}{2}|k|}, \quad k \in \frac{2\pi}{w}\mathbb{Z}. \quad (16)$$

The value $2A_{out} = u_{out}(x = 0^+) - u_{out}(x = w^-)$ for $z = 0$ enters due to an integration by parts in x that removes the derivative on u_{out} .

From (16) one can now read off the profile of the wall tails:

$$m_{out,x} - H = \frac{2A_{out}}{w} \sum_{k \in \frac{2\pi}{w}\mathbb{Z}} \frac{\cos(xk)}{Q + \frac{t}{2}|k|} = \frac{2A_{out}}{Qw} \sum_{n \in \mathbb{Z}} \frac{\cos(2\pi \frac{x}{w} n)}{1 + \frac{\pi t}{Qw}|n|}.$$

Sample No.	Film thickness /nm	$\mu_0 H_a$ /mT	$Q / 10^{-3}$
1	102	2.02	1.36
2	153	1.37	0.93
3	212	1.72	1.16

Table I. Sample properties of extended reference films.

Using $Qw/t \ll 1$, we compute

$$\begin{aligned} m_{out,x} - H &= \frac{2A_{out}}{Qw} \left(1 + \frac{2Qw}{\pi t} \sum_{n=1}^{\infty} \frac{\cos(2\pi \frac{x}{w} n)}{\frac{Qw}{\pi t} + n} \right) \\ &= \frac{2A_{out}}{Qw} \left(1 + \mathcal{O}\left(\frac{2Qw}{\pi t}\right) + \frac{2Qw}{\pi t} \underbrace{\sum_{n=1}^{\infty} \frac{\cos(2\pi \frac{x}{w} n)}{n}}_{=\mathcal{O}(1) + \ln(w/x)} \right) \\ &\approx \frac{2A_{out}}{Qw} \left(1 + \frac{2Qw}{\pi t} \ln \frac{w}{t} \right), \text{ provided } x \sim t. \end{aligned}$$

Equating the inner approximation of the magnetization $m_{in,x}$ in (9) with the outer approximation $m_{out,x}$ from above in the overlapping range we obtain

$$\cos \theta - H \approx \frac{2A_{out}}{Qw} \left(1 + 2 \frac{Qw}{\pi t} \ln \frac{w}{t} \right).$$

The two matching conditions (15) and the above combine to

$$\frac{dE_{core}}{d\theta} + \pi t^2 \frac{2Q \frac{w}{t}}{\pi + 2Q \frac{w}{t} \ln \frac{w}{t}} (\cos \theta - H) (-\sin \theta) = 0.$$

This equation is precisely the first variation of (4) in θ .

Additionally, one computes the domain average of m_x in the periodic case by evaluating the zeroth Fourier mode $\mathcal{F}(m_{out,x} - H)(k = 0) = 2A_{out}/Q$ using the second matching condition:

$$\frac{1}{w} \int_0^w m_{out,x} dx = H + \frac{2A_{out}}{Qw} = H + \frac{\pi}{\pi + 2Q \frac{w}{t} \ln \frac{w}{t}} (\cos \theta - H).$$

Another way of deriving this reduced model consists in studying isolated walls, which decay quadratically for $|x| \gg t/Q$, by similar methods. The superposition of wall tails coming from walls at centers $x \in w\mathbb{Z}$ can be shown to yield the same result as the above Fourier approach.

C. Evaluation of the theoretical results for different material parameters

In the following, we aim to apply the reduced model for interacting tails of asymmetric domain walls using realistic thin film parameters and derive (i) hard axis magnetization curves depending on the domain wall spacing w , (ii) magnetization changes resulting from the Bloch-Néel wall transition under applied magnetic fields and (iii) the contribution of the wall core to the overall magnetization rotation in the walls.

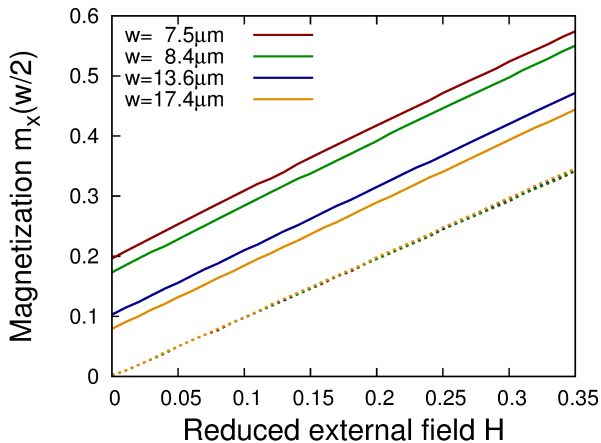


Figure 3. (Color online) Predicted hard-axis magnetization curves for the reduced model (4) with asymmetric Néel cores. The prediction for asymmetric Bloch walls (dotted lines) is essentially independent of domain widths, sample dimensions and material parameters. Material parameters are those of sample 1.

We employ the material parameters shown in Table I which correspond to the samples that will be studied in Section III.

Figure 3 displays the hard-axis magnetization $m_x(w/2)$ that is obtained by minimizing (4) in θ for the material parameters of sample 1 (cf. Table I). The value $m_x(w/2) \approx \cos \alpha_{\text{opt}}$ is obtained from the optimal $\theta = \theta_{\text{opt}}$ in (4) by evaluating (3). As energy of the asymmetric wall core, we use the exchange energy of numerically determined exactly stray-field free asymmetric Bloch and Néel walls, cf. (10). As expected, the choice of material parameters and the tail energy contribution is irrelevant along the Bloch wall branch $m_x(w/2) \approx H$.

As expected, Figure 3 shows that neighboring walls interact more strongly, i.e. entail stronger hysteresis, the narrower the domains are. Note that in the experimentally relevant range of reduced fields $H \in [0, 0.35]$, $m_x(w/2)$ is almost linear in H . Since the instability fields of Néel and Bloch wall seem unavailable within the reduced model, we will therefore use the value $m_x(w/2)$ for zero field $H = 0$ and Néel wall cores to predict the jump $\Delta m_x(w/2)$ between Néel and Bloch magnetization branches at instability.

Figure 4 predicts a strong interaction of neighboring wall tails as soon as the domain period w falls below $\sim 0.2t/Q$. This threshold decreases with increasing reduced film thickness t/d .

Finally, Figure 5 shows the relative amount of rotation $\theta_{\text{opt}}/\alpha$ in wall core and tails for the parameters from samples 1 and 2 in percent as a function of the reduced external field $H \approx 0.3$, in both samples and independent of the domain width, about 90–95% of the rotation falls upon the

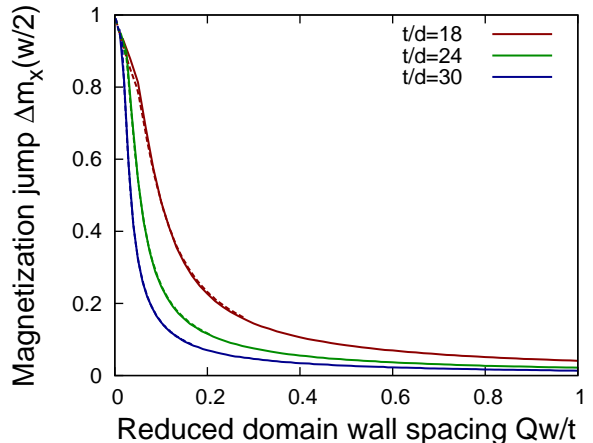


Figure 4. (Color online) The hard-axis magnetization (3) at zero field $H = 0$ for Néel wall cores serves as prediction for the magnetization jump between the almost linear Bloch and Néel wall branches. The curves for amorphous CoFeB (solid lines, $Q = 1.5 \cdot 10^{-3}$) and nanocrystalline Permalloy (dashed lines, $Q = 2.5 \cdot 10^{-4}$) are virtually indistinguishable.

core. At larger fields, the tails gain importance until at fields $H_{AS} \approx 0.75 - 0.9$, depending on the film thickness and domain width, the asymmetric wall core vanishes. The critical field H_{AS} increases with the normalized film thickness t/d , domain width w/t , and inverse anisotropy quality factor $1/Q$. It can be shown to have the value

$$H_{AS} \approx 1 - 4 \frac{\pi + 2Q \frac{w}{t} \ln \frac{w}{t}}{(\frac{t}{d})^2 Q \frac{w}{t}},$$

provided this number is non-negative.

Note that formally, for $w = t/Q$, $Q \ll 1$, we obtain

$$H_{AS} \approx 1 - 8 \left(\frac{d}{t}\right)^2 \ln \frac{1}{Q}$$

as critical field for the transition from asymmetric to symmetric Néel wall in an infinitely extended soft ferromagnetic film without interaction of neighboring wall tails.

III. EXPERIMENTS

In this section, we are going to address the transition between the asymmetric wall types in a varying hard-axis field from an experimental point of view. In particular, we will compare the predicted hard-axis magnetization $m_x(w/2)$ in the domain center (cf. Figure 3) and the magnetization jump $\Delta m_x(w/2)$ (cf. Figure 4) to the corresponding experimental data (cf. Figures 7 and 9).

In fact, the *experimental* observation of strongly hysteretic wall transitions in the presence of nearby walls has originally motivated the *theoretical* study of interacting walls.

Instead of Permalloy, the most popular material used for soft magnetic film studies, we have chosen amorphous

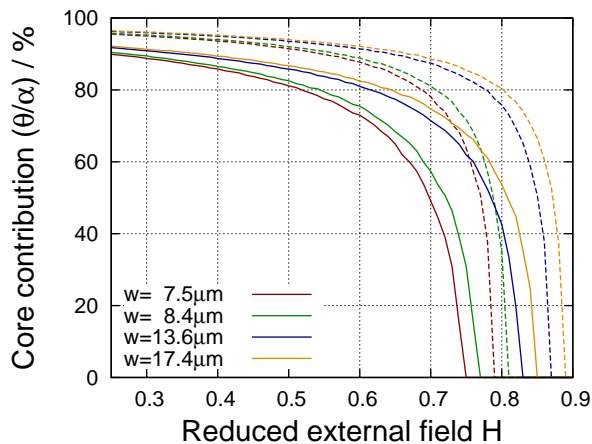


Figure 5. (Color online) A prediction according to (4) of the relative amount of rotation in the asymmetric wall cores for the samples 1 (solid lines) and 2 (dashed lines) for various domain wall spacings, cf. Table I.

CoFeB films for the experimental part. Compared to Permalloy with a typical nanocrystalline microstructure, they have similar magnetic properties, but are lacking significant ripple modulations of magnetization within the domains. The absence of such disturbing inhomogeneity is favorable for subtle domain wall studies.

A. Sample Preparation

Ferromagnetic films of amorphous $\text{Co}_{40}\text{Fe}_{40}\text{B}_{20}$ of varying thicknesses were prepared on glass wafers by means of ultrahigh-vacuum magnetron sputtering at room temperature¹⁹. An in-plane magnetic field of $\mu_0 H_{\text{dep}} = 25 \text{ mT}$ was applied during film deposition to induce a uniaxial magnetic anisotropy. When studying the interaction between adjacent magnetic domain walls one should ideally consider different magnetic domain configurations in *extended* films as the effects of domain wall pinning at domain wall triple junctions and structural edges are reduced¹. However, lateral patterning was found to be required to allow for the creation of well defined magnetic domains with antiparallel magnetization and a narrow distribution of magnetic domain wall spacings. Therefore, arrays of stripe-shaped structures with in-plane dimensions of $60 \mu\text{m} \times 9500 \mu\text{m}$ and the long axis perpendicular to the induced anisotropy axis were patterned using photolithography. A stripe width of $60 \mu\text{m}$ was found to be a good compromise between sufficiently small domain wall spacings and large edge-to-edge-separation. The lateral spacing between individual stripes was chosen to be $90 \mu\text{m}$ to minimize effects originating from interelement magnetostatic interaction. A saturation magnetization of $\mu_0 M_s = 1.48 \text{ T}$ was extracted from out-of-plane magnetization curve measurements of an unpatterned reference film (not shown). Table I summarizes the dif-

ferent samples, including the film thickness and uniaxial anisotropy field $H_a = |\vec{H}_a|$ as derived from in-plane magneto-optical hysteresis measurements along the magnetic hard axis of reference films (not shown). Slight variations of anisotropy strength may be due to slightly different deposition conditions.

B. Magneto-optical Kerr Magnetometry

Flux-closed domain patterns were initialized by demagnetizing the samples in an alternating external magnetic field \vec{H}_{dem} of decreasing amplitude at a frequency of 50 Hz. By varying the in-plane angle α of \vec{H}_{dem} with respect to the anisotropy axis the magnetic domain wall spacing w was systematically altered from broad domain states (for small α) to narrow domain states with small domain wall spacings (for $\alpha \rightarrow 90^\circ$), see exemplarily Fig. 6 (a). The domain states, studied by longitudinal magneto-optical Kerr microscopy¹, comprise basic domains with alternating magnetization direction parallel to the induced magnetic easy axis and a closure structure that consists of easy-axis spike domains and closure domains with \vec{M} parallel to the stripe edges. The vertical bright and dark lines in the domain image with transverse Kerr sensitivity (Fig. 6 (b)) represent the surface magnetization of the 180° -domain walls. From literature^{1,20} and due to the fact that the walls appear equally black and white in the images one can conclude for zero applied field and for the chosen film parameters that these domain walls are asymmetric Bloch walls. A slight mismatch between the induced easy axis of magnetization and the short axis of the elements was introduced during patterning. However, this should not effect the magnetization behavior in hard axis fields in a field range, where closure domains are still present.

Subsequently, a static magnetic field \vec{H} was applied perpendicular to the 180° domain walls, i.e. parallel to the hard axis of magnetization. The domain structure adapts to the increasing hard axis field by rotational magnetization processes inside the basic domains and by growth of the preferentially magnetized (\vec{M} along \vec{H}) closure domains. The evolution of the Kerr intensity parallel to the applied field was recorded for the center area of the basic domains (compare red frame in Fig. 6 (b)). The local magnetization curves of several domains with similar domain wall spacing were averaged and normalized with respect to the Kerr intensity at saturation. As during this hysteresis measurement the maximum applied field amplitude was always smaller than the saturation field of the stripes, any irreversible effects originating from domain nucleation have been reduced. This procedure allows for the local recording of minor domain magnetization curves depending only on the domain wall spacing and the film thickness. Minor domain magnetization loops are demonstrated in Fig. 7 for different domain wall spacings w and

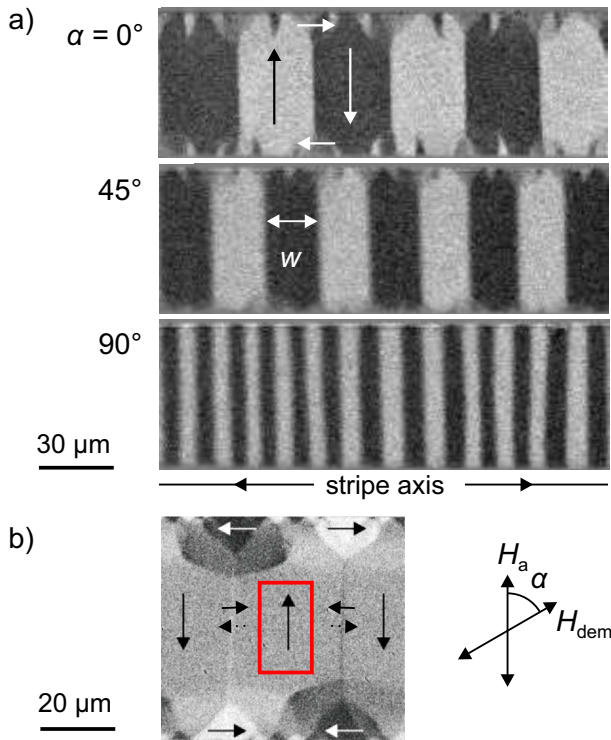


Figure 6. (Color online) a) Kerr images of a stripe section with a thickness of 153 nm after demagnetization with \vec{H}_{dem} under $\alpha = 0^\circ$, 45° and 90° , arrows indicate the magnetization direction within the domains. b) The closure domain state studied with transversal Kerr sensitivity shows that the surface magnetization of neighboring 180° domain walls appears equally dark and bright. Dotted arrows indicate the domain wall magnetization at the bottom surface of the film. In order to extract local magnetization curves only the area highlighted by the red frame was considered.

a film thickness of 102 nm.

For sufficiently small domain wall spacings a jump in the transverse domain magnetization is observed at fields H_{BN} and H_{NB} for increasing and decreasing field, respectively, with $|H_{BN}| > |H_{NB}|$ (see inset in Fig. 7). With decreasing domain wall spacing this hysteresis gets broader and the corresponding jump in the transverse magnetization component increases. Studying the corresponding domain images (see Fig. 8), a superdomain structure appears around H_{BN} which expands progressively from the stripe center towards its edges as the transversal field amplitude is increased.

High resolution imaging of the domain walls (not shown due to weak contrast) revealed that the surface intensity of the former dark domain walls changed to be bright within the area of the brighter superdomains. Consequently, the magnetization jump observed in the local domain magnetization curves under the influence of a transversal magnetic field goes along with the expected transformation of the domain walls from asymmetric Bloch walls to asymmetric Néel walls. This con-

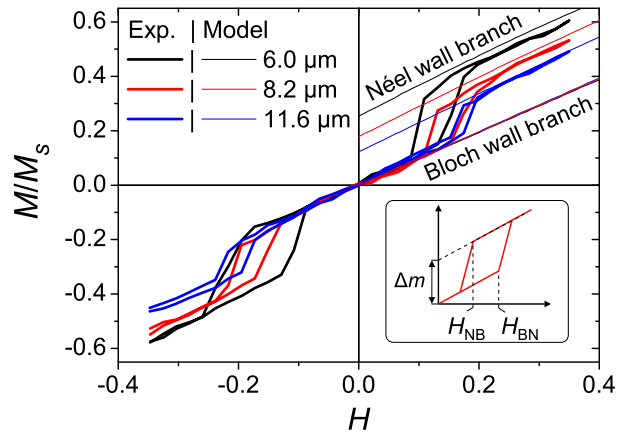


Figure 7. (Color online) Minor magnetization loops for three different basic domain widths measured (thick solid lines) in fields perpendicular to the easy axis of magnetization in a sample of 102 nm thickness. In comparison the calculated hysteresis branches (thin solid lines) for cases of asymmetric Néel walls and asymmetric Bloch walls are shown. The inset schematically illustrates the quantification of the magnetization changes that go along with a wall transformation at transition fields H_{BN} and H_{NB} .

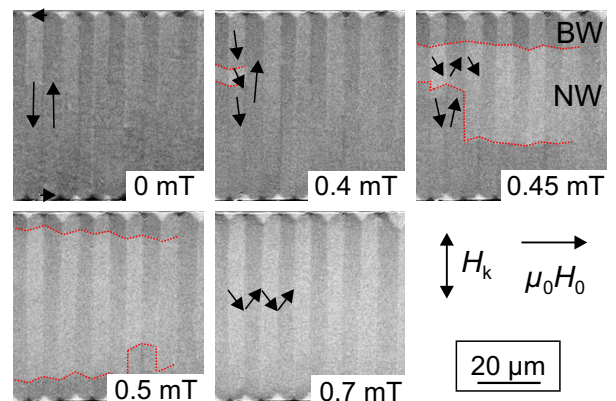


Figure 8. (Color online) Kerr images of a $\text{Co}_{40}\text{Fe}_{40}\text{B}_{20}$ stripe section (thickness: 102 nm). The left image in the first row corresponds to the demagnetized state with \vec{H}_{dem} applied at an angle of $\alpha = 90^\circ$ with respect to \vec{H}_k . Subsequently a transversal field of increasing amplitude is applied as indicated in the domain images. At $\mu_0 H_0 = 0.4$ mT a superdomain structure emerges, which is highlighted by a dotted line for better visibility. The superdomain expands towards the stripe edges as the transversal field amplitude increases. The formation of a superdomain structure is provoked by the transition of the center wall segments from asymmetric Bloch wall (BW) to asymmetric Néel wall (NW).

clusion is supported by the quantitative agreement between the experimental magnetization change and the theoretically predicted magnetization change from the asymmetric Bloch to the asymmetric Néel wall branch (compare thin solid lines in Fig. 7). Upon decreasing the field amplitude the process is reversed (not shown): At

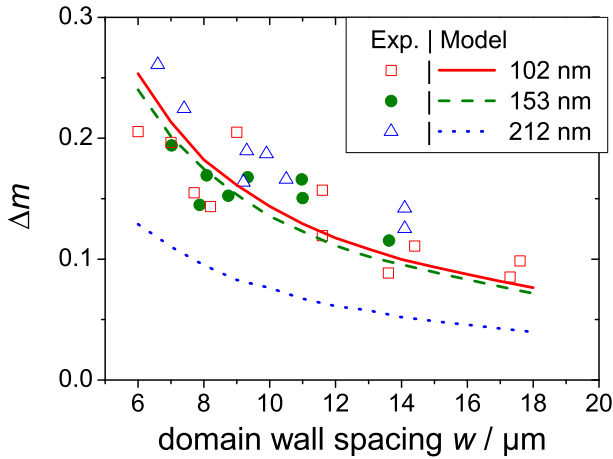


Figure 9. (Color online) Change of the transversal magnetization due to the transition between asymmetric Bloch and asymmetric Néel walls under the action of an applied transversal field. The theoretical values are calculated using the reduced model (4) with experimentally determined material parameters and an exchange constant of $A = 1.3 \times 10^{-11}$ J/m ($d \approx 3.86$ nm for $\mu_0 M_s = 1.48$ T).²¹

a critical field $|H_{NB}| < |H_{BN}|$ darker superdomains appear close to both stripe edges and expand towards the stripe center as H is further decreased. Consequently, H_{BN} corresponds to the reconversion of asymmetric Néel to asymmetric Bloch walls. The jump of the domain magnetization constitutes an additional contribution to the transversal magnetization component due to the interaction of neighboring Néel wall tails. In order to quantify the strength of the interaction between adjacent asymmetric Néel walls for different film thicknesses and domain wall spacings w the magnetization change Δm ($\Delta m_x(w/2)$ in the notation of Section II) was deduced from the corresponding domain magnetization curves as sketched in the inset in Fig. 7. By linearly extrapolating the Néel wall branch of the minor magnetization curves to $H = 0$ the magnetization change due to the wall transition $\Delta m = \frac{M(H=0)}{M_s}$ is quantified independently of the transition fields H_{BN} and H_{NB} , similar to the applied procedure resulting in Fig. 4. Thereby Δm can be compared to the values derived by the presented model where the wall transition fields are not known. Figure 9 compares the experimental and theoretical values of Δm obtained for stripes with a thickness of 102 nm, 153 nm and 212 nm.

As already obvious from Fig. 7 the interaction strength between neighboring Néel wall segments qualitatively increases as the domain wall spacing is reduced which results in an increase of Δm . For a film thickness of 102 nm and 153 nm the experimental values scatter around the theoretical values calculated by using the reduced model (see Sec. II). Hence, quantitative agreement between model and experiment is observed for a film thickness of 102 nm and 153 nm. Whereas the model predicts a slight

decrease of the interaction strength between neighboring Néel wall tails (reduction in Δm) when increasing the film thickness to 212 nm, the experimental values do not follow this trend. On the one hand, this may mean that the reduced model is not suited for the description of domain walls in CoFeB films that exceed a critical thickness. The fact that the samples in Table I do not clearly satisfy the regime $Q(t/d)^2 \ll 1$ might indicate that the breakdown of the reduced model occurs within the range

$$\begin{aligned} 1.5 &\approx 0.93 \cdot 10^{-3} \cdot (153/3.86)^2 \\ &\lesssim Q(t/d)^2 \\ &\lesssim 1.16 \cdot 10^{-3} \cdot (212/3.86)^2 \approx 3.5. \end{aligned}$$

On the other hand, this deviation could be due to slightly varying material parameters for the different depositions, in particular the exchange constant and saturation magnetization. It has been observed that the theoretical predictions of Δm are very sensitive to slight changes of the material parameters.

IV. CONCLUSION

Both, for a single wall in an extended ferromagnetic film as well as a system of interacting domain walls we have reviewed mathematically rigorous reduced models that describe and quantify the splitting of asymmetric domain walls into a stray-field free core and extended logarithmic tails. In addition, the reduced model for interacting walls predicts the average hard-axis magnetization within the domains.

In order to verify the prediction (3), hard-axis magnetization loops for the hysteretic transition between asymmetric Bloch and interacting asymmetric Néel walls have been measured in $\text{Co}_{40}\text{Fe}_{40}\text{B}_{20}$ films of thicknesses 102 nm, 153 nm and 212 nm. While the instability fields for the transition from asymmetric Bloch to Néel wall and vice versa seem inaccessible within the reduced model, it reliably predicts the magnetization curves for asymmetric Bloch and Néel walls in the two thinner samples. In the film of thickness 212 nm, the reduced model underestimates the measured data by a factor of 2, which may indicate that the validity limit of the reduced models can be found within the range $1.5 \lesssim Q(t/d)^2 \lesssim 3.5$.

By evaluating (5) for various field strengths and anisotropies $Q \in \{2.5 \cdot 10^{-4}, 1.5 \cdot 10^{-3}\}$ (corresponding to CoFeB and Permalloy) and determining the energetically favored domain wall among symmetric (characterized by $\theta = 0$) and asymmetric ($\theta > 0$) Néel and asymmetric Bloch walls, we have obtained phase diagrams that qualitatively agree with the previously available results (see Ref. 1, Fig. 3.80). Since the latter are based on numerical simulations, some of them not properly including the effect of extended tails of asymmetric Néel walls, we propose using the reduced models (4) and (5) as an easy-to-use and potentially more precise means of determining

the energy and internal structure of domain walls in ferromagnetic films of medium thickness. In particular, we propose using (5) as wall energy density in domain theory. In this way, employing the well-known ansatz for the cross-tie configuration, also an estimate for the energy of this domain wall microstructure can presumably be obtained.

Furthermore, by presenting a new derivation of the periodic reduced model (4), we demonstrate the equivalence of the energy-^{12,13} and torque-balance based approaches to studying the structure of asymmetric domain walls.

Possible and desirable extensions consist in a verification

of the reduced models and their estimated range of validity in a larger class of samples and ferromagnetic materials, as well as deriving predictions for the instability fields marking the transition between the two asymmetric wall types.

V. ACKNOWLEDGEMENTS

LD acknowledges support of the International Max Planck Research School *Mathematics in the Sciences* and the Max Planck Institute for Mathematics in the Sciences, Leipzig.

* L.Doering@math1.rwth-aachen.de

- ¹ A. Hubert and R. Schäfer, *Magnetic Domains - The Analysis of Magnetic Microstructures*, 1st ed. (Springer, Berlin, Heidelberg, New York, 1998) pp. xxvii+686.
- ² A. Hubert, *Physica status solidi. B, Basic research* **32**, 519 (1969).
- ³ A. Hubert, *Physica status solidi. B, Basic research* **38**, 699 (1970).
- ⁴ C. Hengst, M. Wolf, R. Schäfer, L. Schultz, and J. McCord, *Phys. Rev. B* **89**, 214412 (2014).
- ⁵ R. Kirchner and W. Döring, *Journal of applied physics* **39**, 855 (1968).
- ⁶ H. Riedel and A. Seeger, *Phys. Status Solidi B* **46**, 377 (1971).
- ⁷ C. Melcher, *Arch. Ration. Mech. Anal.* **168**, 83 (2003).
- ⁸ R. Ignat and F. Otto, *J. Eur. Math. Soc. (JEMS)* **10**, 909 (2008).
- ⁹ M. Chermisi and C. B. Muratov, *Nonlinearity* **26**, 2935 (2013).
- ¹⁰ A. LaBonte, *J. Appl. Phys.* **40**, 2450 (1969).
- ¹¹ D. V. Berkov, K. Ramstöck, and A. Hubert, *physica status solidi (a)* **137**, 207 (1993).
- ¹² L. Döring, R. Ignat, and F. Otto, *JEMS* **16**, 1377 (2014).
- ¹³ L. Döring, “A reduced model for asymmetric domain walls with interacting tails in soft ferromagnetic films,” In preparation.
- ¹⁴ A. DeSimone, R. V. Kohn, S. Müller, and F. Otto, in *The Science of Hysteresis*, Vol. 2, edited by G. Bertotti and I. Mayergoyz (Elsevier Academic Press, 2005) Chap. 4, pp. 269–381.
- ¹⁵ F. Otto, in *Proceedings of the International Congress of Mathematicians, Vol. III (Beijing, 2002)* (Higher Ed. Press, Beijing, 2002) pp. 829–838.
- ¹⁶ Due to the limited width of stray-field free walls, $E_{\text{core}}(\theta)$ is accessible to brute-force numerical simulation: First note

that due to the scaling invariance of $\int |\text{grad } \vec{m}|^2 dA$ in two spatial dimensions, it suffices to determine $E_{\text{core}}(\theta)$ for films of non-dimensional thickness 1. Then, a finite-difference approximation of the Euler-Lagrange equation for $E_{\text{core}}(\theta)$ is solved with help of a relaxed Newton method (and PARDISO²² as linear solver), using initial data that resemble asymmetric Néel and Bloch walls. We remark that in contrast to previous studies¹¹ we find that the energy of asymmetric Bloch walls does *increase* with increasing external field. This difference we attribute to a finer resolution of the vortex in the domain wall core. For small domain wall angles $\theta \approx 0$, also a rigorous asymptotic expansion of the wall energy $E_{\text{core}}(\theta) \approx 4\pi \sin^2 \theta + \frac{148}{35} \pi \sin^4 \theta$ (relative error to numerics for stray-field free Néel walls < 15%) and the minimizer is available. The latter confirms the non-monotone rotation of asymmetric Néel walls on the film surface, leading to the experimentally visible double contrast in the wall core. Details can be found in Ref. 23.

- ¹⁷ With a refined ansatz for the bulk energy of the wall tails the scaling of their width $w_{\text{tails}} \sim t/Q$ can actually be derived by this approach.
- ¹⁸ In the single-wall case, one can also read off that the solution $m_{\text{out},x}$ must vary on the scale t/Q , which is the relevant length scale for this equation.
- ¹⁹ Samples were prepared by K. Kirsch at the IPHT Jena with a Cyberite sputtering tool.
- ²⁰ A. Hubert, *Journal of Magnetism and Magnetic Materials* **35**, 249 (1983).
- ²¹ A. Conca, J. Greser, T. Sebastian, S. Klingler, B. Obry, B. Leven, and B. Hillebrands, *J. Appl. Phys.* **113** (2013).
- ²² O. Schenk and K. Gärtner, *Journal of Future Generation Computer Systems* **20**, 475 (2004).
- ²³ L. Döring and R. Ignat, “Asymmetric domain walls of small angle in soft ferromagnetic films,” Submitted.